

Low-Voltage, Compact, Depletion-Mode, Silicon Mach–Zehnder Modulator

Michael R. Watts, William A. Zortman, *Student Member, IEEE*, Douglas C. Trotter, Ralph W. Young, and Anthony L. Lentine

Abstract—Through rigorous process, electrical, and optical simulations, we develop a new silicon depletion-mode vertical p-n junction phase-modulator implemented in Mach–Zehnder modulator configuration, enabling an ultralow measured $V_\pi L$ of only ~ 1 V·cm. Further, in a 500- μm -long lumped element device, we demonstrate a 10-Gb/s nonreturn-to-zero data transmission with wide-open complementary output eye diagrams without the use of signal preemphasis.

Index Terms—Diodes, optical modulation, silicon.

SILICON was first explored as an active optical material by Soref and Bennett [1]. In their seminal publication, Soref and Bennett measured the refractive index of silicon as a function of carrier concentration. Subsequent publications demonstrated useful configurations of silicon modulators [2]–[9]. In terms of the active region of the modulator, these configurations can generally be classified into three categories: 1) injection mode [2]–[4], [9]; (2) MOS-capacitors [7], [8]; and 3) depletion-mode structures [4]–[6], [10]. The full-optical structure can then be generally classified as Mach–Zehnder [2]–[7] or resonant modulators [9], [10]. Mach–Zehnder modulators have the benefit of wideband operation, and hence greatly reduced temperature sensitivity. Resonant structures greatly enhance the relatively weak free-carrier effect, thereby enabling ultralow power consumption [9], but operate only over a narrow bandwidth and suffer from substantial temperature sensitivities. Both structures have merit; however, we consider here Mach–Zehnder implementations only.

Injection-based silicon modulators [2]–[4], [9] have the capability to induce a large change in the free-carrier concentration at a relatively low voltage. The figure of merit, $V_\pi L$, for injection-based modulators has been reported to be as low as 0.02 V·cm [3]. However, injection-based modulators suffer from the long free-carrier lifetime (~ 1 ns) in silicon-on-insulator (SOI) silicon. As a result, the 3 dB bandwidths of injection-based modulators are typically below 1 GHz [3]. To achieve higher speed operation, signal preemphasis has been success-

fully utilized [9], but doing so requires complex circuitry, higher drive voltages, and higher power consumption.

Silicon p-n junction modulators can, of course, be run in depletion mode, where carriers are extracted rather than injected [4]–[6] and high-speed operation (30 GHz) has been obtained. However, without a p-n junction tailored to run in depletion mode in a tightly confined structure, these structures suffer from very small changes in refractive index, resulting in substantially reduced figures of merit (i.e., $V_\pi L = 4$ V·cm [4], $V_\pi L = 5$ V·cm [5]) compared to forward-biased operation.

Alternatively, the free-carrier lifetime limitation in silicon can be overcome by the use of a MOS capacitor structure [7], [8]. MOS capacitor structures are in some ways much like p-n junctions, except they are formed from three distinct layers: a poly-Si layer, an oxide layer, and an SOI silicon layer. By applying a voltage, carriers can either be stored onto the capacitor or depleted from the poly-Si and SOI silicon layers. In either case, a refractive index change is induced. Modulators with 3 dB bandwidths exceeding 20 GHz have been achieved in MOS capacitor Mach–Zehnder modulators, but at relatively high figures of merit, $V_\pi L \sim 3.3$ V·cm [8]. In principle, MOS capacitors can achieve low figures of merit when run in accumulation mode without free-carrier lifetime limitations. The benefits of MOS capacitor modulators stem from the high field and large degree of charge accumulation that can be achieved in MOS capacitor structures [11]. However, MOS capacitors generally require a poly-Si layer that can introduce excess loss.

Here, we develop a simple depletion-based vertical p-n junction, similar to that used for our resonant modulator [10], [12], [14] for a Mach–Zehnder configuration. This junction enables a substantially improved modal overlap of the depletion region with the propagating mode enabling shorter structures with improved figures of merit (i.e., lower $V_\pi L$, where V_π is the voltage required to achieve a π phase shift at a device length L). Here, we demonstrate a figure of merit of $V_\pi L = \sim 1$ V·cm. In a simple, lumped element configuration, we achieve “error-free” (i.e., bit error rate $< 10^{-12}$) 10-Gb/s nonreturn-to-zero (NRZ) data transmission and a 3-dB electrical bandwidth of 8 GHz limited only by the impedance of the 50 Ω transmission line used to drive the modulator.

I. MODULATOR DESIGN

A. Depletion-Mode p-n Junction Design

The parameters describing a depletion-mode modulator design can be arrived at by considering the effect of free carriers on the refractive index and the extent to which free carriers can be

Manuscript received June 6, 2009; revised July 8, 2009. Current version published February 5, 2010. This work was supported by Sandia’s Laboratory Directed Research and Development Program.

M. R. Watts, D. C. Trotter, R. W. Young, and A. L. Lentine are with Sandia National Laboratories, Albuquerque, NM 87185 USA (e-mail: mwatts@sandia.gov; dctrott@sandia.gov; rwyong@sandia.gov; allenti@sandia.gov).

W. A. Zortman is with Sandia National Laboratories, Albuquerque, NM 87185 USA, and also with the Center for High Technology Materials, University of New Mexico, Albuquerque, NM 87131 USA (e-mail: wzortm@sandia.gov).

Color versions of one or more of the figures in this paper are available online at <http://ieeexplore.ieee.org>.

Digital Object Identifier 10.1109/JSTQE.2009.2035059

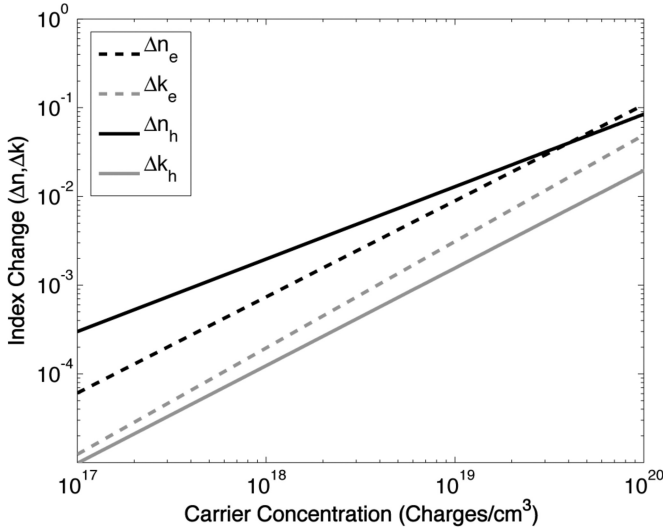


Fig. 1. Change in the real and imaginary components of the refractive index are plotted as a function of carrier concentration for both electrons and holes at a wavelength of $\lambda = 1550$ nm. The change in the real part of the refractive index is larger than that of the imaginary part and impacted more greatly by holes. The plots were obtained from curve fits to the experimental data reported in [1].

depleted. The refractive index change (Δn) stems from results of Soref and Bennett [1], which at a wavelength of $\lambda = 1550$ nm in silicon are described as follows:

$$\Delta n = A \cdot N^B + jC \cdot N^D \quad (1)$$

where N is the electron (N_e) or hole (N_h) free-carrier concentration and the curve fitting parameters $A_e = -2.4 \times 10^{-22}$, $B_e = 1.1$, $C_e = 4.9 \times 10^{-26}$, and $D_e = 1.2$, and $A_h = -3.9 \times 10^{-18}$, $B_h = 0.8$, $C_h = 2 \times 10^{-24}$, and $D_h = 1.1$, are used for the electrons and holes, respectively. The results of (1) are plotted in Fig. 1.

From Fig. 1, we observe that the change in the refractive index is small for both the electrons and the holes. Additionally, of the two, holes provide a larger change in refractive index Δn and a smaller change in the imaginary index Δk for a given change in free-carrier concentration. As a result, it is desirable to minimize the overlap of the optical field with electrons and maximize the overlap with the depletion of holes. In depletion-mode operation, the change in the effective index of propagation is determined by the overlap of the field with the refractive index change. It is therefore desirable to maximize the fractional change in guide depletion. From the depletion approximation [13] given by

$$w = \sqrt{\frac{2\varepsilon N_A + N_D}{q N_A N_D} (V + \phi_B)} \quad (2)$$

where w is the depletion width, ε is the dielectric constant, q is the electron charge, V is the applied voltage, ϕ_B is the built-in potential, and N_D and N_A are the donor and acceptor concentrations, we see that the depletion width is inversely proportional to the square root of the carrier concentration and directly proportional to the square root of the applied voltage. Given that we desire to achieve a large fractional change in depletion width across the guide with a high concentration of free carriers, the

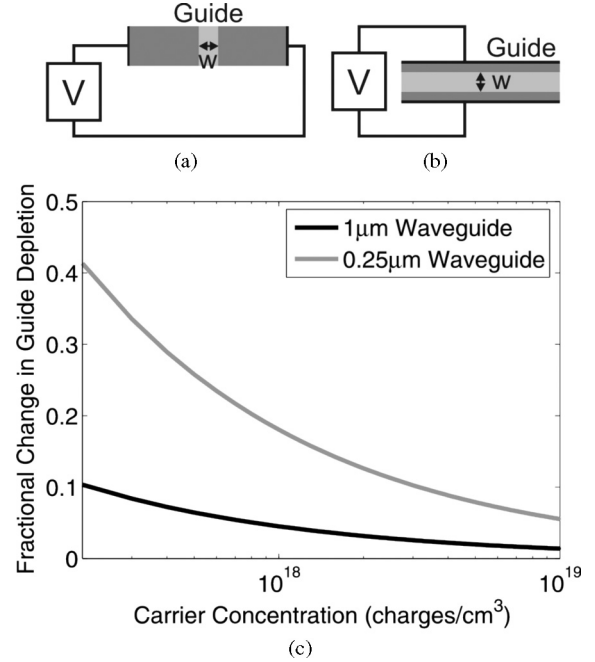


Fig. 2. Cross-sectional diagrams of modulators formed by applying voltages across the (a) wide and (b) narrow gaps of waveguides, and (c) a plot of the fractional change in the waveguide depletion obtained from the depletion approximation [13] extending from 0 to 2.5 V applied for a 0.25- μm silicon waveguide and a 1- μm waveguide. The fractional change in depletion is greater than a factor of 4, which is better for the narrow guide with a vertical junction. This figure was originally presented in [14].

guide width (or height) must be kept small. Generally, it is easier to form a wide, rather than tall, waveguide. Therefore, at a given carrier concentration, vertical p-n junctions achieve larger fractional changes in depletion, and hence larger changes in the effective refractive index. This effect is depicted in Fig. 2.

B. Finite-Element Modeling Results

From the simple considerations presented in the previous section, we developed a baseline vertical p-n junction modulator structure [see Fig. 3(a)]. The structure is formed from a 60-nm ridge on top of a 180-nm SOI slab. The vertical p-n junction is formed by implanting the n and p regions with different implant energies, and electrical contact to the junction is made with tungsten vias connected to p+ and n+ plugs. Full-process and 2-D finite-element electrical device simulations were performed using Synopsys Tsupreme and Medici processing and electrical simulation tools, with the dopant distributions generated from implant energies and doses similar to those provided in Section II.A. The contact separation of 2.8 μm was chosen so as to minimize the device resistance while maintaining low-loss operation. The resistance and capacitance of the structure per unit length were calculated at a bias of 2.5 V to be 6.7 $\text{k}\Omega \cdot \mu\text{m}$ and 0.83 $\text{fF}/\mu\text{m}$, respectively, enabling an intrinsic RC time constant of 5.6 ps or a 3-dB bandwidth, $1/(2\pi RC)$, of 29 GHz.

Under no applied bias, the built-in internal field of the junction partially depletes the junction. The remaining carriers contribute to approximately 2.7dB/mm of propagation loss obtained by inserting the carrier concentrations obtained from the process and electrical simulations into a finite-difference mode solver

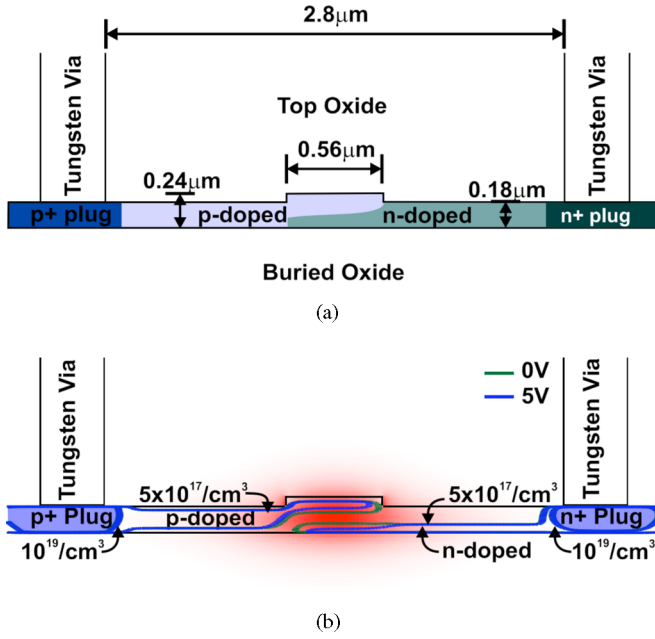


Fig. 3. (a) Cross-sectional diagram of the vertical p-n junction active region of the phase modulator. (b) Combined finite-element process/electrical and finite-difference optical simulations of the active region of the modulator as a function of the applied voltage. The simulations indicate that a phase change of π rad can be achieved at an applied reverse-bias voltage of ~ 5 V and device length of ~ 2.2 mm, and a wavelength of $\lambda = 1.55 \mu\text{m}$ or a $V_{\pi}L = 1.1$ V·cm. The dopant concentrations are shown using contour plots for both 0 (green) and 5 V (blue) applied, while the amplitude of the electric field of the optical mode is shown in red.

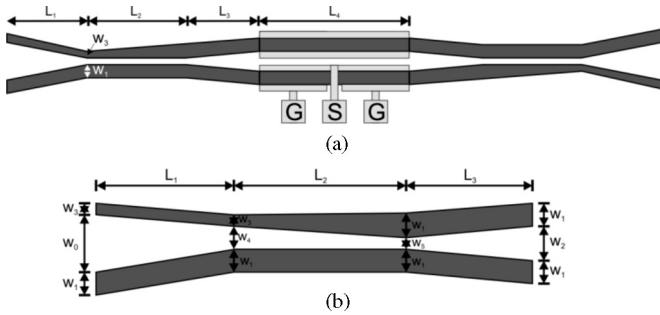


Fig. 4. Diagram of the (a) Mach-Zehnder modulator structure and (b) a closeup of the adiabatic coupler region. The adiabatic couplers enable a four-port coupler with complementary outputs to be achieved. In this regard, the Mach-Zehnder modulator is as much a high-speed switch as it is a modulator. The dimensions of the structure are as follows; $w_1 = 0.6 \mu\text{m}$, $w_2 = 10 \mu\text{m}$, $w_3 = 0.4 \mu\text{m}$, $w_4 = 0.8 \mu\text{m}$, $L_1 = 1$ mm, $L_2 = 0.5$ mm, and $L_3 = 0.5$ mm.

simulation. Under an applied bias of 5 V, the loss is reduced to 1.65 dB/mm and a phase change of 1.4 rad/mm is predicted for a figure of merit of $V_{\pi}L = 1.1$ V·cm at a device length of 2.2 mm.

C. Mach-Zehnder Design

The Mach-Zehnder structure was formed with a pair of four-port adiabatic couplers providing complementary output ports for use in differential signaling, or alternatively, high-speed switching. The basic structure is shown in Fig. 4(a).

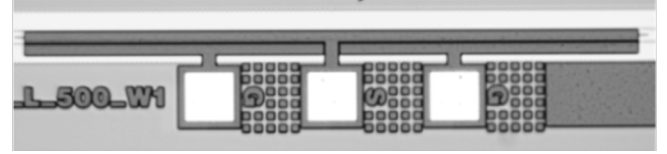


Fig. 5. Optical micrograph of the active portion of our 500- μm -long silicon Mach-Zehnder modulator. The GSG probe pads are prominently shown.

The use of adiabatic couplers in a silicon Mach-Zehnder modulator was previously demonstrated by Spector *et al.* [4]. Adiabatic couplers ensure broadband operation with relatively loose fabrication tolerances. A closeup of the four-port coupler is depicted in Fig. 4(b). For simplicity, the modulator was designed as a lumped element device without traveling wave electrodes. As such, the realized bandwidth of the device is expected to be limited to the RC time constant of the full structure and experimental setup. The 50Ω transmission line used to drive the modulator will limit the 3-dB bandwidth to a predicted 6.3 GHz, as a result of the increased impedance induced by the 50Ω transmission line, rather than the intrinsic RC time constant of the active region (29 GHz).

II. FABRICATION AND EXPERIMENTAL RESULTS

A. Fabrication

The modulator geometry shown in Fig. 3 was fabricated on a 6-in-diameter SOI substrate with 250 nm of silicon on $3 \mu\text{m}$ of buried oxide. The waveguide and ridge geometry was patterned with an ASML deep UV (248 nm) laser scanner and subsequently etched with reactive ion etching. The silicon layer was then oxidized down to a total thickness of 240 nm. The p-n junctions were formed by implanting $4 \times 10^{13}/\text{cm}^2$ arsenic (Ar) and $2.87 \times 10^{13}/\text{cm}^2$ boron-flourine (BF_2) atoms/molecules using 380 and 110 KeV energies, respectively, directed from the four cardinal wafer directions (commonly called a quad implant) at a 7° tilt to minimize ion channeling in the silicon lattice. Using these dopants and energies after the ridge has been etched produces a vertical p-n junction with $\sim 10^{18}/\text{cm}^3$ free-carrier concentration while providing a conductive path back to the contacts. The contact area was doped using $2 \times 10^{15}/\text{cm}^2$ phosphorus (P) and $10^{15}/\text{cm}^2$ (BF_2), again using a quad 7° wafer tilt and energies of 40 and 35 KeV, respectively. Contact was then made using standard 500-nm-wide tungsten plugs through a ~ 0.9 - μm -deposited tetra-ethyl oxy-silicate (TEOS) oxide layer. Aluminum lines and pads were subsequently defined and etched. Final passivation was performed with phospho-silicate glass (PSG). An optical micrograph of a fabricated 500- μm -long Mach-Zehnder modulator is shown in Fig. 5.

B. Experimental Results

The fabricated structures were tested to determine their dc and high-frequency characteristics. A parameter of critical importance is the device figure of merit, $V_{\pi}L$. To determine the figure of merit accurately, both output ports of the Mach-Zehnder modulator were carefully measured. The phase angle

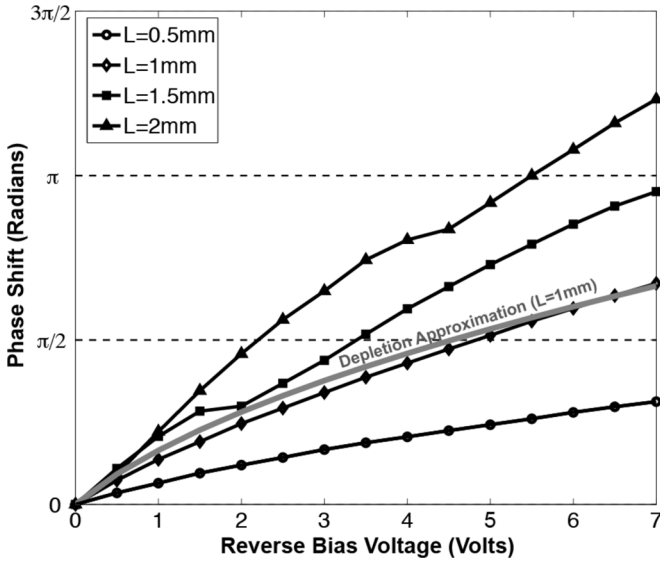


Fig. 6. Derived phase shifts for 0.5-, 1.0-, 1.5-, and 2.0-mm-long active region Mach-Zehnder modulators obtained by measuring both output ports of the four-port Mach-Zehnder modulators at a wavelength of $\lambda = 1.5 \mu\text{m}$. The measured result for $L = 1 \text{ mm}$ is compared against that obtained from the depletion approximation (2) using equal donor and acceptor carrier densities of $10^{18}/\text{cm}^3$, demonstrating close agreement between theory and experiment.

θ required to simultaneously produce the measured outputs in each port was then determined by comparing the power out of both the bar and cross ports (i.e., P_{bar} and P_{cross}) using the output power relations of a standard four-port Mach-Zehnder interferometer. The relationship between θ , P_{bar} , and P_{cross} is described by (3), which is accurate for the small amount of differential loss exhibited in the two arms of these Mach-Zehnder modulators

$$\theta = \cos^{-1} \left(\frac{P_{\text{cross}} - P_{\text{bar}}}{P_{\text{bar}} + P_{\text{cross}}} \right). \quad (3)$$

In Fig. 6, the phase angle as a function of applied voltage was derived using (3) and the measured outputs of 0.5-, 1-, 1.5-, and 2-mm-long active region Mach-Zehnder modulators. The average experimentally determined phase shift per millimeter of device length was found to 1.53 rad at 5 V, demonstrating a $V_{\pi}L \cong 1 \text{ V}\cdot\text{cm}$ for a 2-mm device length, a new record published figure of merit for a depletion-mode silicon Mach-Zehnder modulator. The phase shifts at both $\lambda = 1.5 \mu\text{m}$ and $\lambda = 1.55 \mu\text{m}$ were found to be in very close agreement.

In addition to the phase shifts, the losses were compared between the different length active regions. Doing so, we measured a loss of 3.1 dB/mm in the active region with 0 V applied at a wavelength of $\lambda = 1.5 \mu\text{m}$. The losses decreased to 2 dB/mm with 5 V applied bias due to the decrease in the free-carrier concentration caused by depletion. At a wavelength of $\lambda = 1.55 \mu\text{m}$, the losses increased by $\sim 1 \text{ dB/mm}$ due to increased interaction with the n+ and p+ plug implants for the more weakly confined field. The cause of the increased loss was confirmed by measuring the losses in structures with an increased contact

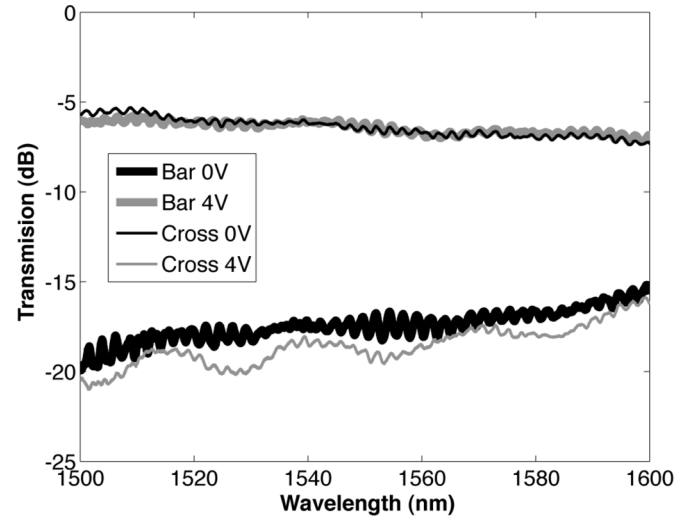


Fig. 7. Measurement of the bar and cross port outputs of a 2-mm-long Mach-Zehnder modulator with 0 and 4 V applied.

separation of $3.8 \mu\text{m}$. In these, otherwise, identical structures, the loss at $\lambda = 1.55 \mu\text{m}$ was measured to be 3 dB/mm at 0 V and 1.8 dB/mm at 5 V, demonstrating close agreement with our numerically predicted losses of 2.7 and 1.65 dB/mm at 0 and 5 V, respectively. The required increased contact separation at $\lambda = 1.55 \mu\text{m}$ is believed to be a result of a slightly smaller than expected ridge height obtained from fabrication and not a fundamental issue with the design. Both the measured phase change and the measured losses closely agree with the numerical results obtained through a combination of process simulations and electromagnetic mode solver calculations. The slight disparity in phase shift and loss are likely a result of the minor differences between the simulated and physically applied implants, and slight differences in the fabricated versus simulated geometries.

To demonstrate the dc characteristics of the structure, the output ports of a 2-mm-long device were measured with 0 and 4 V applied bias. The results are shown in Fig. 7. Over 14 dB extinction is obtained in both the bar and cross ports by applying this relatively small applied bias.

The electrical bandwidth of the 500- μm -long device was determined by the use of a time-domain-reflectometry (TDR) measurement. The measured electrical spectral response at both 0 and 2.5 V was plotted in Fig. 8. The electrical S_{11} response indicates 3- and 8-GHz 3-dB bandwidths at the two bias points. The 2.5 V applied bias has a higher electrical bandwidth due to the reduced capacitance in the partially depleted junction. Since the rate of carrier extraction is directly related to optical modulation, the electrical S_{11} response should be a very close indicator of the modulator bandwidth, and is in close agreement with the predicted RC time constant of the modulator in series with the 50Ω transmission line of 6.3 GHz. With the addition of a traveling wave electrode, which would provide an impedance match, or alternatively, a low impedance electrical drive, the device speed should approach the intrinsic bandwidth

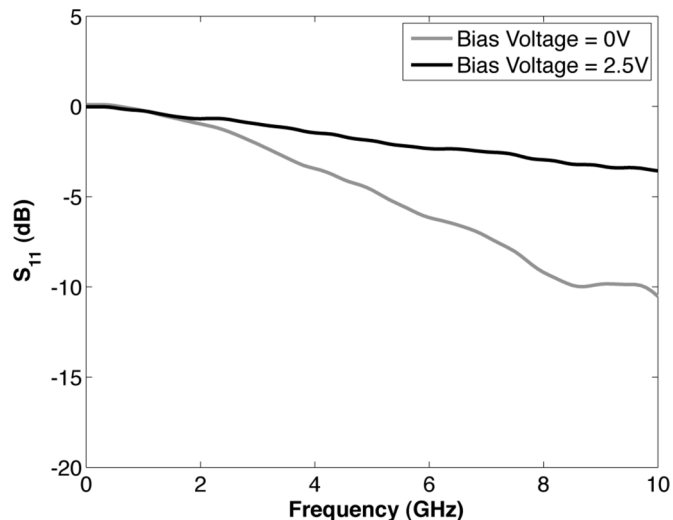


Fig. 8. TDR measurement of S_{11} indicating the electrical bandwidth of a modulator with a 500- μm -long active region for 0 and 2.5 V applied reverse bias.

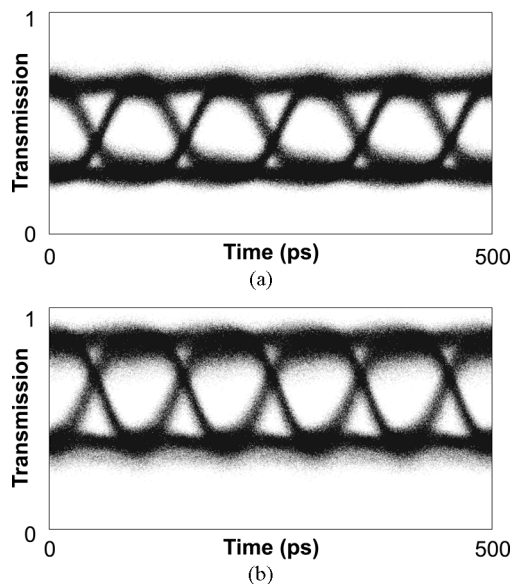


Fig. 9. Eye diagrams of the (a) cross and (b) bar output ports of the 500- μm -long Mach-Zehnder Modulator with a peak-to-peak 5-V drive without using signal preemphasis. In each case, BERs below 10^{-12} were measured for PRBS of $2^{23} - 1$ pattern lengths.

of the junction (29 GHz), and provide sufficient bandwidth for 40 Gb/s NRZ data transmission.

Still, even without traveling wave electrodes, the 500- μm -long device has adequate bandwidth for a 10-Gb/s NRZ data transmission. Eye diagrams of both output ports of the modulator obtained from the modulator with a 10-Gb/s NRZ pseudorandom bit stream (PRBS) with a 2.5-V reverse bias and peak-to-peak amplitude of 5 V with a pattern length of $2^{23} - 1$ are presented in Fig. 9, and the BER was measured to be below 10^{-12} . The device was driven with a ground-signal-ground (GSG) 50 Ω terminated probe.

III. CONCLUSION

From simple geometric considerations stemming from the depletion approximation, we have developed a silicon depletion-mode phase modulator that maximizes the overlap of the depletion region with the optical mode enabling a π phase shift with only 5 V applied to be achieved in a ~ 2 -mm-long structure, thus realizing a $V_{\pi}L$ of only ~ 1 V \cdot cm. Further, in a 500- μm -long lumped element device, we demonstrate a 10-Gb/s NRZ data transmission with wide-open complementary output eye diagrams and without the use of signal preemphasis. The measured 3-dB electrical bandwidth of the modulator was measured to be ~ 8 GHz, limited only by the RC time constant of the 50- Ω transmission-line-driven lumped element. Future improvements, such as the inclusion of traveling wave electrodes and more aggressive doping schemes, will likely enable even higher bandwidth (>40 GHz) operation with even lower $V_{\pi}L$ figures of merit.

ACKNOWLEDGMENT

The authors would like to thank M. Popovic for use of his finite-difference electromagnetic mode solver.

REFERENCES

- [1] R. A. Soref and B. R. Bennett, "Electrooptical effects in silicon," *IEEE J. Quantum Electron.*, vol. QE-23, no. 1, pp. 123–129, Jan. 1987.
- [2] F. Gan and F. X. Kärtner, "High-speed silicon electrooptic modulator design," *IEEE Photon. Technol. Lett.*, vol. 17, no. 5, pp. 1007–1009, May 2005.
- [3] G.-R. Zhou, M. W. Geis, S. J. Spector, F. Gan, M. E. Grein, R. T. Schuelein, J. S. Orcutt, J. U. Yoon, D. M. Lennon, T. M. Lyszczarz, E. P. Ippen, and F. X. Kärtner, "Effect of carrier lifetime on forward-biased silicon Mach-Zehnder modulators," *Opt. Exp.*, vol. 16, pp. 5291–5226, Apr. 2008.
- [4] S. J. Spector, M. W. Geis, G.-R. Zhou, M. E. Grein, F. Gan, M. A. Popović, J. U. Yoon, D. M. Lennon, E. P. Ippen, F. X. Kärtner, and T. M. Lyszczarz, "CMOS-compatible dual-output silicon modulator for analog signal processing," *Opt. Exp.*, vol. 16, pp. 11027–11031, Jul. 2008.
- [5] A. Liu, L. Liao, D. Rubin, H. Nguyen, B. Ciftcioglu, Y. Chetrit, N. Izhaky, and M. Paniccia, "High-speed optical modulation based on carrier depletion in a silicon waveguide," *Opt. Exp.*, vol. 15, no. 2, pp. 660–668, 2007.
- [6] L. Liao, A. Liu, D. Rubin, J. Basak, Y. Chetrit, H. Nguyen, R. Cohen, N. Izhaky, and M. Paniccia, "40 Gbit/s silicon optical modulator for high speed applications," *Electron. Lett.*, vol. 43, no. 22, pp. 1196–1197, Oct. 2007.
- [7] A. Liu, R. Jones, L. Liao, D. Samara-Rubio, D. Rubin, O. Cohen, R. Nicolaescu, and M. Paniccia, "A high-speed silicon optical modulator based on a metal-oxide-semiconductor capacitor," *Nature*, vol. 427, pp. 615–618, 2004.
- [8] L. Liao, D. Samara-Rubio, M. Morse, A. Liu, and D. Hodge, "High-speed silicon Mach-Zehnder modulator," *Opt. Exp.*, vol. 13, pp. 3129–3135, 2005.
- [9] Q. Xu, S. Manipatruni, B. Schmidt, J. Shakya, and M. Lipson, "12.5 Gbit/s carrier-injection-based silicon microring silicon modulators," *Opt. Exp.*, vol. 15, pp. 430–436, 2007.
- [10] M. R. Watts, D. C. Trotter, R. W. Young, and A. L. Lentine, "Ultralow power silicon microdisk modulators and switches," in *Proc. IEEE 2008 Int. Meeting Group IV Photon.*, Sorrento, Italy, Sep., pp. 4–6.
- [11] T. L. Koch, private communication, 2009.
- [12] M. R. Watts, D. C. Trotter, and R. W. Young, "Maximally confined high-speed second-order silicon microdisk switches," presented at the Opt. Fiber Commun. Conf. (OFC) Nat. Fiber Opt. Eng. Conf. (NFOEC), San Diego, CA, 2008, Paper PDP14.
- [13] A. S. Grove, *Physics and Technology of Semiconductor Devices*. New York: Wiley, 1967, ch. 6.
- [14] M. R. Watts, D. C. Trotter, R. W. Young, A. L. Lentine, and W. A. Zortman, "Limits to silicon modulator bandwidth and power consumption," presented at the Proc. SPIE Photon. West, San Jose, CA, 2009.

Michael R. Watts received the B.Sc. degree in electrical engineering from Tufts University, Medford, MA, in 1996, and the M.Sc. and Ph.D. degrees in electrical engineering from Massachusetts Institute of Technology, Cambridge, in 2001 and 2005, respectively.

From 1996 to 1999, he was a member of the Technical Staff at Draper Laboratories, Cambridge, MA, and from 1999 to 2001, he was a Draper Fellow. In 2005, he joined the Technical Staff at Sandia National Laboratories, Albuquerque, NM, where he is currently a Principal Member of the Technical Staff with Sandia's Applied Photonic Microsystems Department. He has authored or coauthored more than 30 conference and journal publications, various invited talks and papers, two book chapters, and five U.S. patents in microphotonic devices and systems.

Dr. Watts is a member of the Optical Society of America (OSA). He was a member on the committees of the IEEE Group IV Photonics, OSA Integrated Photonics and Nanophotonics Research and Applications, and the Conference on Lasers and Electro-Optics.

William A. Zortman (S'07) received the Bachelor's degree in atmospheric science from the University of Arizona, Tucson, and the M.S. degree in electrical engineering in 2008 from the University of New Mexico, Albuquerque, where he is currently working toward the Ph.D. degree in electrical engineering with Center for High Technology Materials.

Currently, he is interning at Sandia National Laboratories' Applied Photonic Microsystems Department, Albuquerque.

Mr. Zortman is a student member of the Optical Society of America.

Douglas C. Trotter joined Sandia National Laboratories, Albuquerque, NM, in 2007, where he is currently a member of the Microelectronics Development Laboratory's CMOS Department, with focus on the process integration and manufacture of photonic devices.

During 1976, he was with Philips Semiconductors. He has been involved with the development of bipolar, CMOS, and BiCMOS technologies.

Ralph W. Young received the B.Sc. degree in physics and the Ph.D. degree in solid-state physics from Brigham Young University, Provo, UT, in 1974 and 1978, respectively.

From 1978 to 2002, he was with IBM Microelectronics Division, Fishkill, NY, where he was involved in practicing process and device simulations of bipolar and field-effect transistor technologies. In 2002, he joined Sandia National Laboratories, Albuquerque, NM, as a Principal Member of the Technical Staff, where he continues to practice simulations of a variety of semiconductor devices. He is the author or coauthor of more than 20 technical papers. He holds ten U.S. patents.

Anthony L. Lentine received the Bachelor's and M.Sc. degrees in electrical engineering from the University of Illinois, Urbana, in 1979 and 1980, respectively, and the Ph.D. degree from Heriot-Watt University, Edinburgh, U.K., in 1993.

He was a Senior Director of Optical and System Engineering with Ciena Corporation, a Founder and the Chief Scientist with Internet Photonics Incorporated, and a Distinguished Member of the Technical Staff with Bell Laboratories, Lucent Technologies, and AT&T. Since 2007, he has been a Principal Member of the Technical Staff with the Applied Photonic Microsystems Department, Sandia National Laboratories, Albuquerque, NM. He was involved with advances in telecommunications, data communications, optical interconnects, and optical logic.

He has authored or coauthored more than 60 refereed papers, more than 100 conference publications, 4 book chapters, and 26 issued U.S. patents.

Dr. Lentine is a member of the Photonics Society of the IEEE. He is a member on the committee for the IEEE Workshop in Interconnections within Digital Systems.